

Seismic Performance of Precast Segmental Bridges: Segment-to-Segment Joints Subjected to High Flexural Moments and Low Shears

Sami Megally, Ph.D.

Assistant Project Scientist
Department of Structural Engineering
University of California at San Diego
La Jolla, California



Frieder Seible, Ph.D., P.E.

Dean of Jacobs School of Engineering and
Professor of Structural Engineering
University of California at San Diego
La Jolla, California

Robert K. Dowell, Ph.D., P.E.

Principal
Dowell-Holombo Engineering, Inc.
San Diego, California
and
Assistant Adjunct Professor
Department of Structural Engineering
University of California at San Diego
La Jolla, California



A three-phase research project is currently in progress to investigate the seismic performance of precast segmental concrete bridges. This paper presents experimental and analytical results of the first phase, which focused on segment-to-segment joints subjected to high flexural moments and low shears. Four large-scale units were tested under fully reversed cyclic displacements. The major test variable was the ratio of internal to external post-tensioning of the superstructure. This paper also presents results of nonlinear finite element modeling of the test units. All test units could undergo significant seismic displacements and joint openings before failure. It was found that the use of external tendons improves ductility and displacement capacity and minimizes permanent displacements and permanent openings of segment-to-segment joints. It was also found that internally bonded and external (unbonded) tendons should not be combined in high seismic zones.

Precast segmental bridge construction has many advantages over the conventional cast-in-place construction method. However, the popularity of precast segmental bridges in high seismic zones is hampered because of severe restrictions on their construction.

The AASHTO Guide Specifications for Design and Construction of Segmental Concrete Bridges,¹ referred to as the AASHTO Guide Specifications throughout this paper, per-

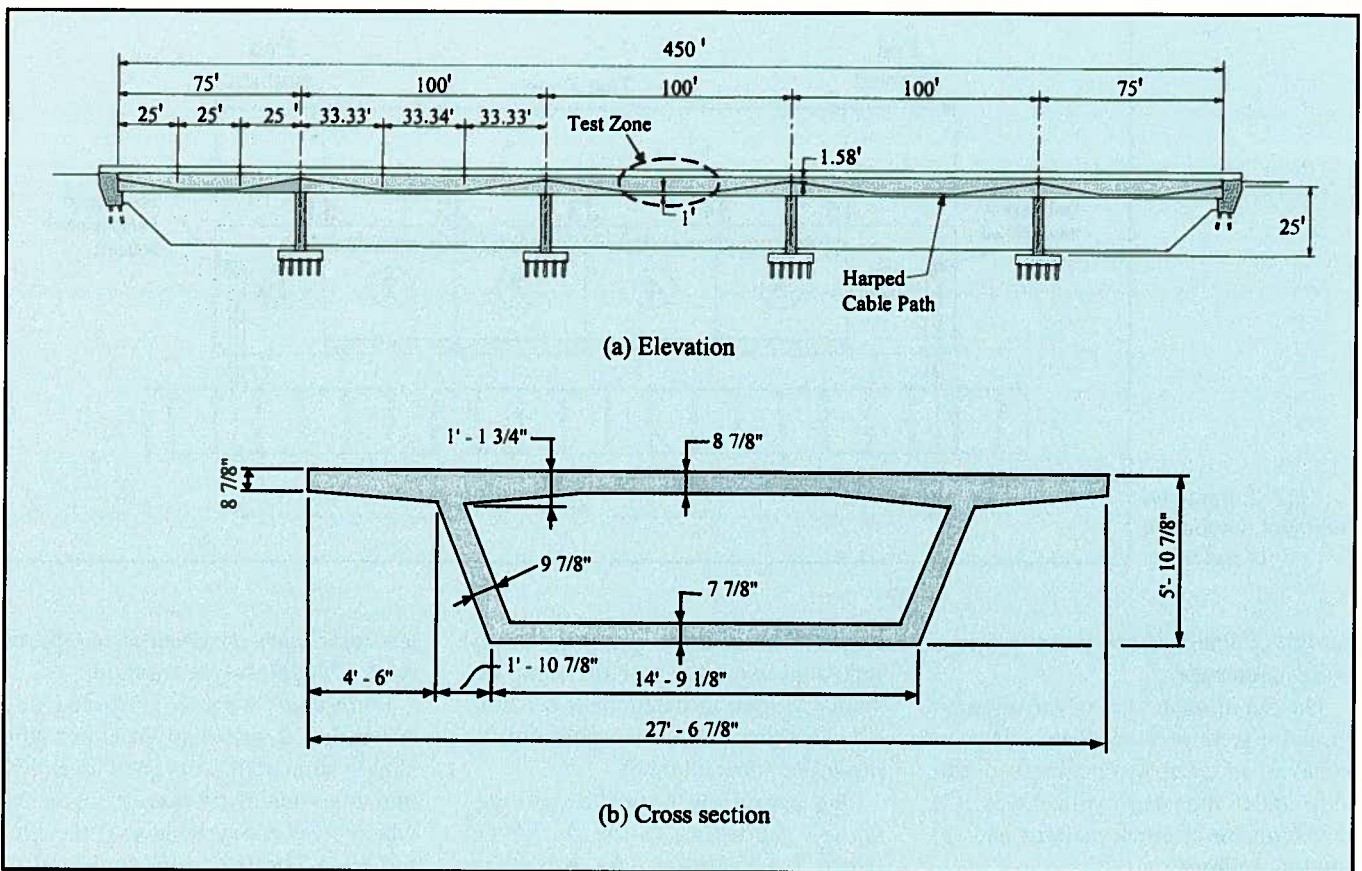


Fig. 1. Prototype structure: (a) Elevation; and (b) Cross section.

mits the use of precast segmental construction in high seismic zones (Zones C and D) provided that the precast segments are epoxy bonded. The same AASHTO Guide Specifications¹ also requires that external (unbonded) tendons shall provide not more than 50 percent of the total post-tensioning.

This requirement was not based on any experimental or analytical evidence but was adopted in the second edition of the AASHTO Guide Specifications¹ to match the current policy of the California Department of Transportation (Caltrans). In addition, precast segmental bridge construction without mild steel reinforcement crossing the segment-to-segment joints is not recommended in current practice in high seismic zones such as California.

The above-mentioned recommendations and restrictions of current practice are justified due to lack of experimental research data regarding seismic performance of precast segmental bridges. Thus, a comprehensive research project has been developed by ASBI (American Segmental Bridge

Institute), Caltrans and the University of California at San Diego (UCSD) to investigate the seismic performance of precast segmental bridges. The large-scale experimental research project is currently in progress at UCSD. This research project is funded by Caltrans and it consists of the following three phases:

- **Phase I:** To investigate the seismic performance of segment-to-segment joints in superstructures with different ratios of internal to external post-tensioning. Only superstructure joints close to midspan in regions with high positive flexural moments and low shears were considered in this phase. Phase I consists of the following two parts:

- (1) **Phase I-A:** Superstructures with 100 percent internal post-tensioning (Test Units 100INT and 100INTCIP; see Table 1).

- (2) **Phase I-B:** Superstructures with different ratios of internal to external post-tensioning (Test Units 100INT, 100EXT and 50INT/50EXT). Test Units 100EXT and 50INT/50EXT were identical to Test Unit 100INT,

with the only difference being the percentage of external post-tensioning. Test Unit 100EXT, with 100 percent external post-tensioning, does not satisfy the current requirement of the AASHTO Guide Specifications¹ that not more than 50 percent of post-tensioning should be achieved by external tendons.

- **Phase II:** To investigate the seismic performance of superstructure segment-to-segment joints close to the supports in regions with high shears and negative flexural moments.

- **Phase III:** To investigate the performance of superstructure-column systems under gravity loads combined with seismic forces. Seismic performance of cast-in-place and precast segmental hollow rectangular columns will also be investigated in Phase III.

The first two phases of the project have been completed, whereas the third phase is currently in progress. Results of Phase I-A test units were presented in an earlier paper,² while experimental and analytical results of Phase I-B are presented in this paper. The experimental and finite element

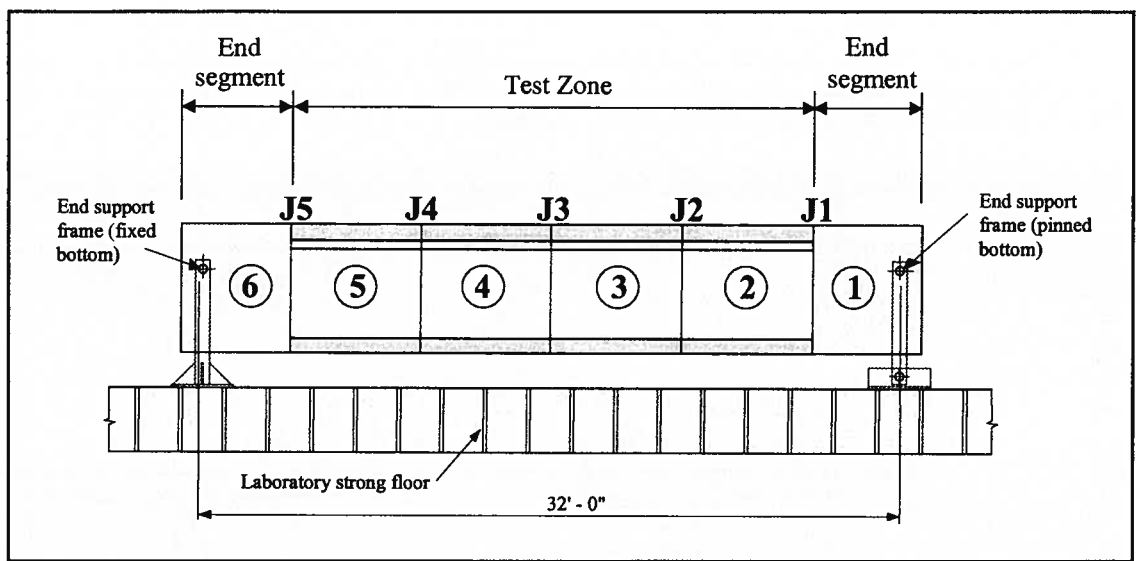


Fig. 2. Joint and segment numbering of test units.

results of Phase II are presented in a companion paper.³

The major objectives of the research program were to investigate: (1) joint behavior in terms of opening and closure under repeated cyclic loads, (2) development of crack patterns and (3) modes of failure.

As part of the research project, three-dimensional finite element models of the test units were developed. The models allowed for concrete cracking and crushing, opening and closure of segment-to-segment joints and inelastic characteristics of prestressed and nonprestressed steels. The finite element models were validated with the experimental results presented in this paper.

The main objective of the analytical models described in this paper is to capture important characteristics of joint behavior. These finite element results will be used in Phase III of the research project to aid development of several comprehensive global finite element bridge models to be used for analytical parametric studies.

PROTOTYPE STRUCTURE

Test units of Phase I of this experimental program are based on the prototype structure shown in Fig. 1. The superstructure consists of three 100 ft (30.48 m) interior spans and 75 ft (22.86 m) exterior spans with a total length of 450 ft (137.2 m). The superstructure is post-tensioned with harped-shape tendons (see Fig. 1a).

Because of its short spans, the prototype superstructure is built using the span-by-span construction method. Fig. 1b shows the cross section of the prototype superstructure.

The prototype structure was designed according to the AASHTO Guide Specifications,¹ the AASHTO-PCI-ASBI Segmental Box Girder Standards for Span-by-Span and Balanced Cantilever Construction,⁴ and the AASHTO Standard Specifications for Highway Bridges.⁵ More details about the design of the prototype structure are given elsewhere.⁶

EXPERIMENTAL PROGRAM

This section gives a description of the Phase I test units and method of construction as well as the test setup and loading sequence. While construction of the test units and setup have been described in an earlier paper,² they are repeated here for completeness.

Description of Test Units

The critical location of the prototype structure for positive flexural moment under dead load and seismic forces was found to be approximately at midspan.⁶ This is because onset of joint opening under the combined effects of dead load, longitudinal and vertical seismic forces was determined to occur near the midspan.⁶ The test units model the middle third of an interior prototype span in which the tendons are horizontal (see Fig. 1a). The

test units were designed at two-thirds scale of the prototype structure.

Four units were constructed and tested. Fig. 2 shows a typical test unit, simply supported at its ends. Each test unit consisted of six precast segments, which were epoxy bonded at their interfaces. The test zone consisted of four 6 ft (1.83 m) long by 4 ft (1.22 m) deep precast segments (Segments 2 to 5 in Fig. 2). Each test unit was supported at its ends by precast end segments (Segments 1 and 6 in Fig. 2).

Fig. 3 shows the cross section and reinforcement of precast Segments 2 through 5 (see Fig. 2) in the Phase I-B test units. Half of the prototype box girder superstructure section was modeled and idealized in the shape of an equivalent I-section to simplify the test setup.

The test matrix is given in Table 1. A total of four units were built and tested; the test units were grouped into two phases, or two test series. Test Series I-A (Phase I-A) consisted of two test units (Units 100INT and 100INTCIP, Table 1). The test variable in Phase I-A was the presence of mild steel reinforcement crossing the segment-to-segment joints. Experimental and finite element analysis results of the Phase I-A test units were presented in an earlier paper² as mentioned previously.

This paper is concerned with Test Series I-B (Phase I-B), which consisted of two test units (Units 100EXT and 50INT/50EXT) in addition to Test Unit 100INT of Phase I-A; the latter was the control specimen of the Phase

I test series. The test variable in Phase I-B was the ratio of internal to external post-tensioning (see Table 1 and Fig. 3). The internally bonded tendon provided 100 percent of the post-tensioning in Test Unit 100INT.

Unit 100EXT was identical to Unit 100INT except that two external (unbonded) tendons, placed symmetrically about the centerline of the web, provided 100 percent of the post-tensioning (see Fig. 3). Thus, Unit 100EXT did not satisfy the AASHTO Guide Specifications requirement that not more than 50 percent of post-tensioning should be provided by external tendons in high seismic zones.¹

An internally bonded tendon provided 50 percent of the post-tensioning in Unit 50INT/50EXT, with the remaining 50 percent provided by two external (unbonded) tendons (see Fig. 3). Thus, Unit 50INT/50EXT satisfied the above-mentioned AASHTO Guide Specifications' upper limit for the allowable percentage of external post-tensioning.¹

Sikadur 31, SBA (Segmental Bridge Adhesive) slow-set epoxy was used for bonding of the precast segments of each test unit. For Units 100INT, 100EXT and 50INT/50EXT, the epoxy was applied to the entire cross section of the segment-to-segment joints. Specifications of the epoxy are given in Table 2, in which σ_{comp} and σ_{bond} are the compressive and bond strengths, respectively.

Each test unit was post-tensioned with sixteen 0.6 in. (15.2 mm) diameter strands with an ultimate tensile strength of 270 ksi (\approx 1860 MPa). The prestressing force was equal for all test units and was calculated so that the concrete stresses resulting from post-tensioning were the same as for the prototype structure.

Table 2 gives the measured concrete material properties of the Phase I-B test units. In Table 2, f'_c is the concrete compressive strength on the day of testing.

Construction of Test Units

As mentioned above, each test unit consisted of six precast segments. Segments 1, 3 and 5 (see Fig. 2) were cast at the same time. This was fol-

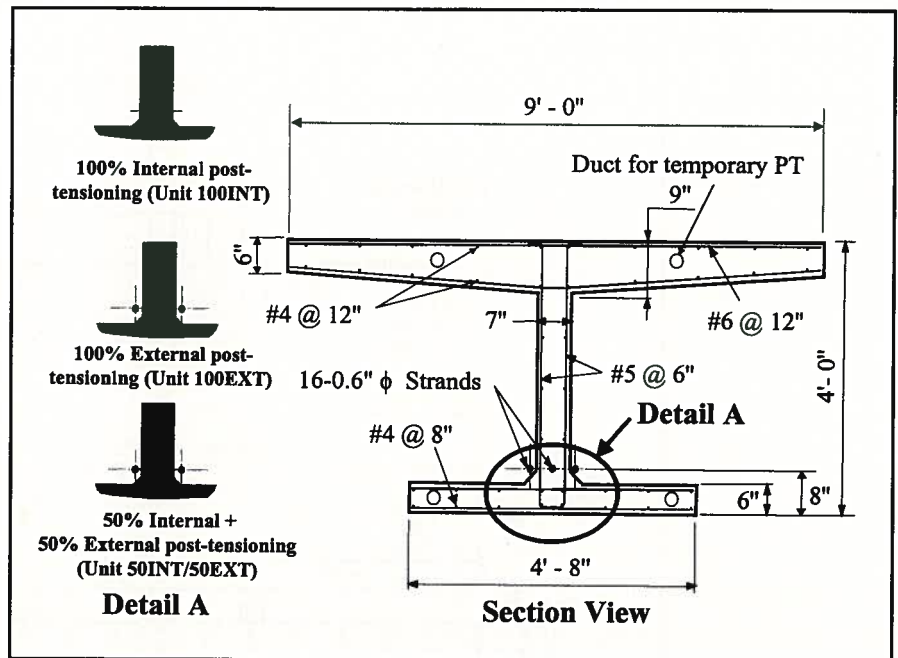


Fig. 3. Cross section of test units (Phase I-B).

Table 1. Test matrix.

Phase (Test series)	Test unit number	Test unit designation	Test unit description
I-A*	1	100INT	100% Internal post-tensioning
	2	100INTCIP	100% Internal post-tensioning and cast-in-place deck closure joints
I-B†	1	100INT	100% Internal post-tensioning
	3	100EXT	100% External post-tensioning
	4	50INT/50EXT	50% Internal + 50% External post-tensioning

* Results of the Phase I-A test units were presented in Reference 2.

† Phase I-B consists of Test Units 100EXT and 50INT/50EXT in addition to Test Unit 100INT of Phase I-A.

Table 2. Material properties.

Test unit	f'_c (on day of testing)			Epoxy properties* (Sikadur 31, SBA) ksi (MPa)	
	ksi (MPa)			σ_{comp} (3 days)	σ_{bond} (14 days)
	Segment No. 1 & 5	Segment No. 3	Segment No. 2, 4 & 6		
100INT	5.11 (35.2)	7.21 (49.7)	6.96 (48.0)	2.0 (13.8)	1.0 (6.9)
100EXT	5.92 (40.8)	5.92 (40.8)	6.79 (46.8)	2.0 (13.8)	1.0 (6.9)
50INT/50EXT	8.01 (55.2)	8.01 (55.2)	6.17 (42.6)	2.0 (13.8)	1.0 (6.9)

* Epoxy properties are those specified by the manufacturer (slow-set epoxy).

lowed by construction of Segments 2, 4 and 6, which were match-cast against Segments 1, 3 and 5.

The segments of each test unit were assembled on a wooden platform at the UCSD Structures Laboratory. The epoxy was applied to the joint surfaces. After application of the epoxy and placement of each segment in its final position, the test unit was temporarily post-tensioned by means of high-strength ASTM A 722 prestressing steel bars.² The temporary pre-

stressing forces in the high-strength bars were determined so that the entire segment-to-segment joint surfaces would have a minimum compressive stress of 40 psi (0.28 MPa).⁷

After epoxy bonding of the precast segments, each test unit was post-tensioned with a jacking force of 720 kips (3203 kN). The effective prestressing force at time of testing was estimated, by hand calculations and computer time-step analyses, to be about 600 kips (2669 kN). The difference be-

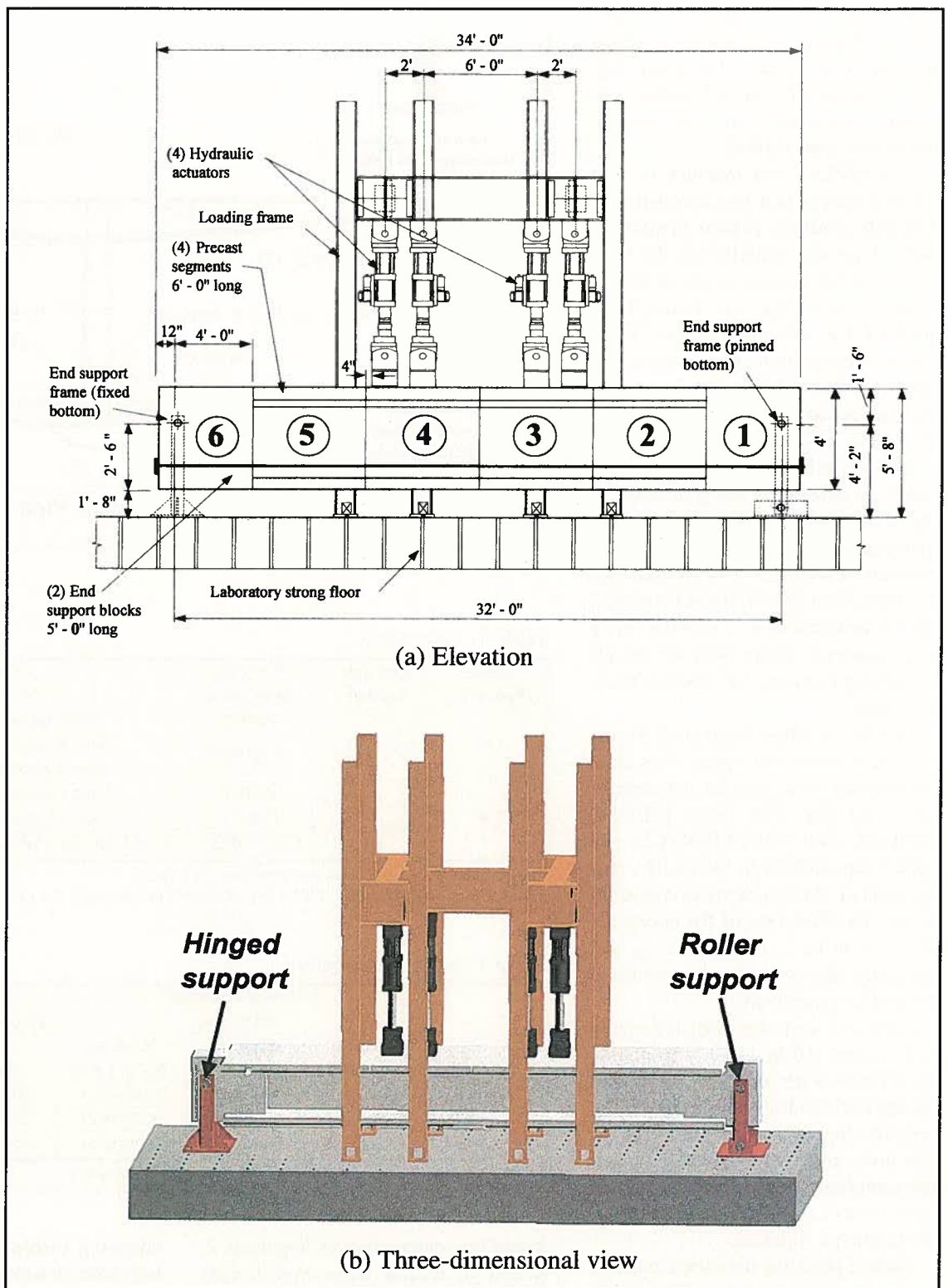


Fig. 4. Test setup:
 (a) Elevation; and
 (b) Three-dimensional view.

tween jacking and effective prestressing forces was due to losses from anchor set, elastic shortening, creep and shrinkage of the concrete as well as relaxation of the prestressing steel.

The temporary prestressing force in the bottom slab was released after permanent post-tensioning of the test unit, whereas the temporary prestress-

ing force in the top slab was released only after vertical loading of the test unit was applied to simulate prototype dead load stresses. The stressing and loading sequence was designed to avoid cracking of the units before the test. After permanent post-tensioning, the wooden platform, supporting the segments during assembly, was re-

moved and the test unit was mounted on the two end supports.

Test Setup

Fig. 4a shows a schematic elevation view of the test unit and the load frame. Each test unit was simply supported by a steel pin and steel links at

its ends. At one end, the steel links were fixed at their bottom ends to restrain horizontal movement of the test units. At the other end, the steel links were pinned at their bottom ends (rocker links) to allow rotation of the frame legs and horizontal expansion and contraction movements of the test units. The loads were transferred from the test units to the steel links by means of steel pins set inside horizontal steel pipes that were cast into the end segments at the neutral axis of the test units, allowing the ends of the test units to rotate freely.

Four vertical servo-controlled hydraulic actuators were used to apply external loads to each test unit to simulate the effect of highway loading and vertical seismic displacements on the superstructure. Fig. 4b shows a pictorial drawing of the test setup. As at the midspan joint of the prototype span, the midspan joint of each test unit was subjected to zero shearing force and the highest flexural moment.

At the beginning of the test, each unit was loaded in the downward direction to a prescribed level so that the stresses at the midspan joint were equal to the prototype structure stresses under combined dead load, superimposed dead load, as well as prestressing primary and secondary effects. This load level is referred to as the reference load level throughout this paper. Each test was conducted as follows:

Stage I (Service Load Conditioning) — Only the two interior actuators were used in load control during this test stage. Each test unit was loaded to the reference load level at $P = 74.5$ kips (331 kN), where P is the load per each actuator. The temporary prestressing force in the top slab was released at this stage.

Cycling the load P between 112 and 65 kips (498 and 289 kN) 100,000 times followed this. The upper and lower load limits provided the same midspan stresses as the prototype structure under maximum and minimum service loads.² This testing stage was performed to investigate the effects of service loading on seismic performance of the superstructure.

Stage II (Seismic Test) — All four actuators were used in displacement

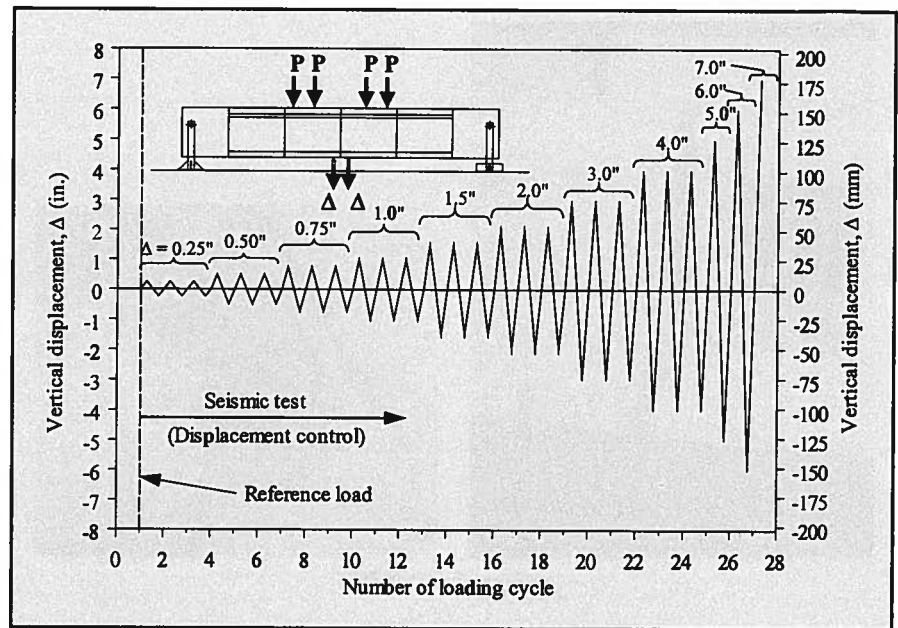


Fig. 5. Loading protocol of the seismic test (Test Stage II).

control with actuator forces maintained equal throughout this test stage. Each test unit was loaded to the reference load level of $P = 40.5$ kips (180 kN) per actuator, or a total load of 162 kips (721 kN). Each test unit was then subjected to fully reversed cyclic vertical displacements at midspan with increasing amplitude to failure.

For each target displacement up to 4 in. (102 mm) magnitude, three cycles were completed. Beyond 4 in. (102 mm) displacements, only one cycle was performed at each displacement level. The displacement history during the seismic test (Test Stage II) is shown in Fig. 5.

Electrical resistance gauges were used to measure strains in the concrete and prestressing steel. Vertical displacements along the span, joint openings at various locations, vertical sliding between the precast segments at each joint and support displacements were measured by means of linear potentiometers.

EXPERIMENTAL RESULTS

The major experimental results are presented in this section. These experimental results include crack patterns, modes of failure, load-displacement response, performance of joints, strains in prestressing steel, stresses in external tendons and flexural moment capacity.

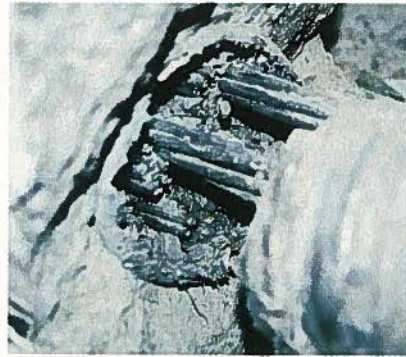
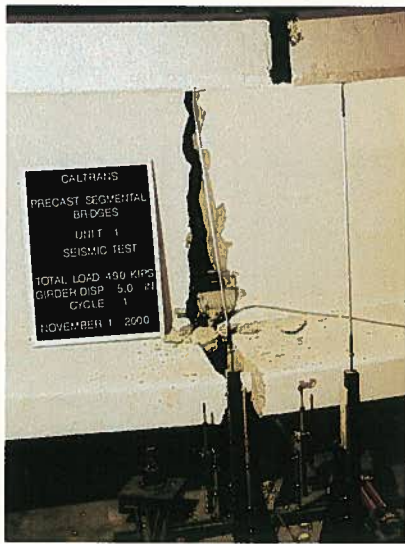
Crack Patterns and Modes of Failure

All test units were subjected to very low tensile stresses at the midspan joint during Test Stage I (Service Load Conditioning).² Thus, no joint openings were observed in any of the test units during Test Stage I; because of this linear-elastic behavior of the test units, only the results of the seismic tests (Test Stage II) will be discussed here.

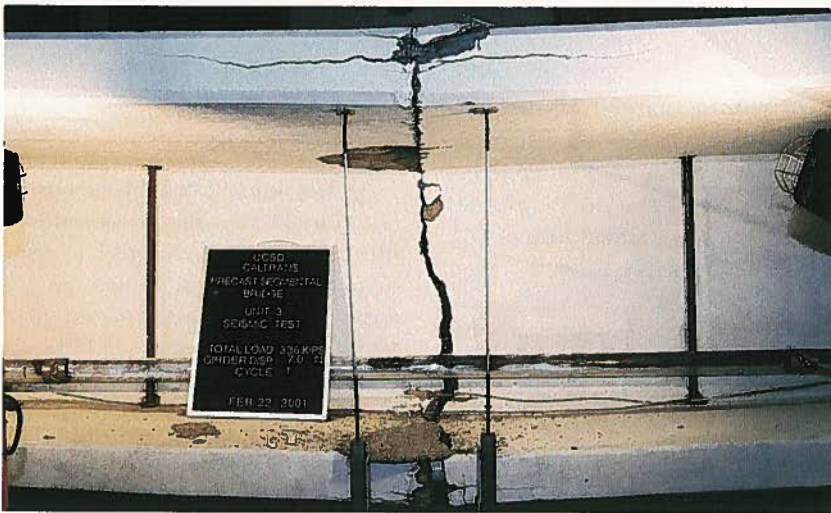
Test Unit 100INT — The first crack occurred under downward loading at the midspan joint (Joint J3, Fig. 2) during the first loading cycle to 0.25 in. (6.35 mm) displacement (see Fig. 5). Opening of Joint J4 (see Fig. 2) also occurred during the same displacement cycle. The midspan total displacement at onset of cracking of Joints J3 and J4 was 0.30 in. (7.62 mm). The total displacement is the sum of the seismic displacement (see Fig. 5) and the displacement at the reference load level (≈ 0.11 in. = 2.79 mm).

Joint J2 (see Fig. 2) opened under downward loading during the 0.5 in. (12.7 mm) displacement cycle. The midspan total displacement at onset of Joint J2 opening was 0.53 in. (13.5 mm). Thus, the three interior Joints J2, J3 and J4 (see Fig. 2) opened during downward loading.

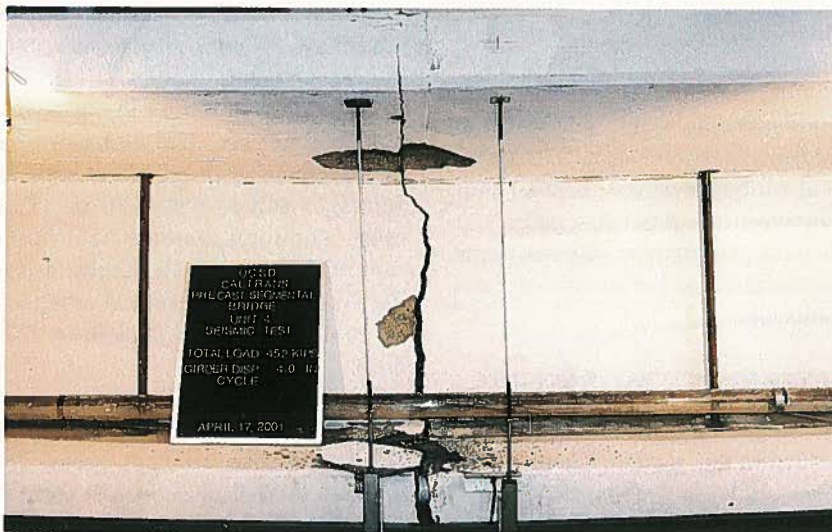
A few additional flexural cracks oc-



(a) Test Unit 100INT



(b) Test Unit 100EXT



(c) Test Unit 50INT/50EXT

Fig. 6. Failure at the midspan joint: (a) Test Unit 100INT; (b) Test Unit 100EXT; and (c) Test Unit 50INT/50EXT.

curred inside Segments 3 and 4 (see Fig. 2) during subsequent downward loading cycles. However, the widths of these cracks were very small and inelastic deformations of the test unit were concentrated mainly at midspan Joint J3.

Midspan Joint J3 was the only joint that opened during upward loading of Unit 100INT, and joint opening occurred during the 0.5 in. (12.7 mm) displacement cycle. Because Unit 100INT did not have any mild steel reinforcement crossing the joints, the opening of midspan Joint J3 increased significantly under upward loading during subsequent displacement cycles.²

Shear cracks occurred in the web under downward loading between the supported ends of the test unit and the load application points (zero shearing force at midspan). Shear cracks crossed the epoxy-bonded joints with no vertical sliding between adjacent precast segments.

Under downward loading, the midspan Joint J3 opened significantly with increased applied displacement until rupture of the prestressing strands at the midspan joint at a displacement of about 4.8 in. (122 mm) and a total load of 490 kips (2180 kN). Fig. 6a shows the midspan joint after failure of Test Unit 100INT, as well as a close-up view of the ruptured strands.

Test Unit 100EXT — The first crack occurred under downward loading at the midspan joint (Joint J3, Fig. 2) during the first cycle to 0.25 in. (6.35 mm) displacement (see Fig. 5). The total midspan displacement at onset of Joint J3 cracking was about 0.32 in. (8.13 mm). During subsequent loading cycles, widening of Joint J3 was observed with no openings in any of the other joints.

Midspan Joint J3 was also the only joint that opened during upward loading of Unit 100EXT. Joint J3 opened under upward loading during the 0.5 in. (12.7 mm) displacement cycle; a drop in the overall load occurred after this. During the 2.0 in. (50.8 mm) upward displacement cycle, the bottom slab came into contact with the external tendons; the load carrying capacity increased during subsequent upward

Table 3. Summary of test results.

Test unit	P_u^* kips (kN)	Δ_u^* in. (mm)	Δ_r^\dagger in. (mm)	Δ_r/Δ_{Ref}	ζ^\ddagger (percent)	ζ/ζ_{Ref}	M_{Test}^* kip-ft (kN-m)	M_{Calc}^* kip-ft (kN-m)	M_{Test}/M_{Calc}
100INT	490 (2180)	4.8 (122)	1.17 (29.7)	8.36	4.21	1.60	3126 (4238)	2993 (4058)	1.04
100INTCIP	480 (2135)	5.9 (150)	0.53 (13.5)	3.79	8.75	3.33	3062 (4151)	2974 (4032)	1.03
100EXT	417 (1855)	6.6 (168)	0.14 (3.56)	1.00	2.63	1.00	2688 (3644)	2732 (3704)	0.98
50INT/50EXT	451 (2006)	4.1 (104)	0.82 (20.8)	5.86	3.87	1.47	2894 (3924)	2867 (3887)	1.01

* Values given for downward loading direction.

† Δ_r and ζ were determined for the 3 in. (76.2 mm) displacement cycle.

loading cycles as a result of this contact. There were no adverse effects of the bottom slab bearing on the external tendons.

Shear cracks occurred in the web under downward loading in Segments 2 and 5 only (see Fig. 2); there were significantly fewer shear cracks than observed for all other test units, which had internally bonded tendons. No shear cracks were observed inside Segments 3 and 4 (see Fig. 2).

Onset of concrete deck crushing occurred during the 4 in. (102 mm) downward displacement cycle. A peak downward load of 417 kips (1855 kN) was attained at a midspan displacement of 3.53 in. (89.7 mm). Unlike the explosive failure resulting from rupture of strands in Unit 100INT, the load carrying capacity of Unit 100EXT dropped gradually with each displacement cycle beyond the peak load.

The test was terminated at a midspan downward displacement of about 6.6 in. (168 mm), when the displacement capacity of the hydraulic actuators was reached. Fig. 6b shows the midspan joint of Unit 100EXT at the maximum displacement level reached during the test.

Test Unit 50INT/50EXT — Performance of Unit 50INT/50EXT was similar to that of Unit 100INT. The first crack was observed inside Segment 3 at about 15 in. (381 mm) away from the midspan Joint J3 (see Fig. 2); this crack occurred during the first downward displacement cycle to 0.25 in. (6.35 mm) amplitude.

Opening of the midspan Joint J3 occurred under downward loading during the first cycle to 0.5 in. (12.7 mm) displacement. The total midspan displacement at onset of Joint J3 cracking was about 0.49 in. (12.4 mm). Opening of Joints J2 and J4 (see Fig. 2) oc-

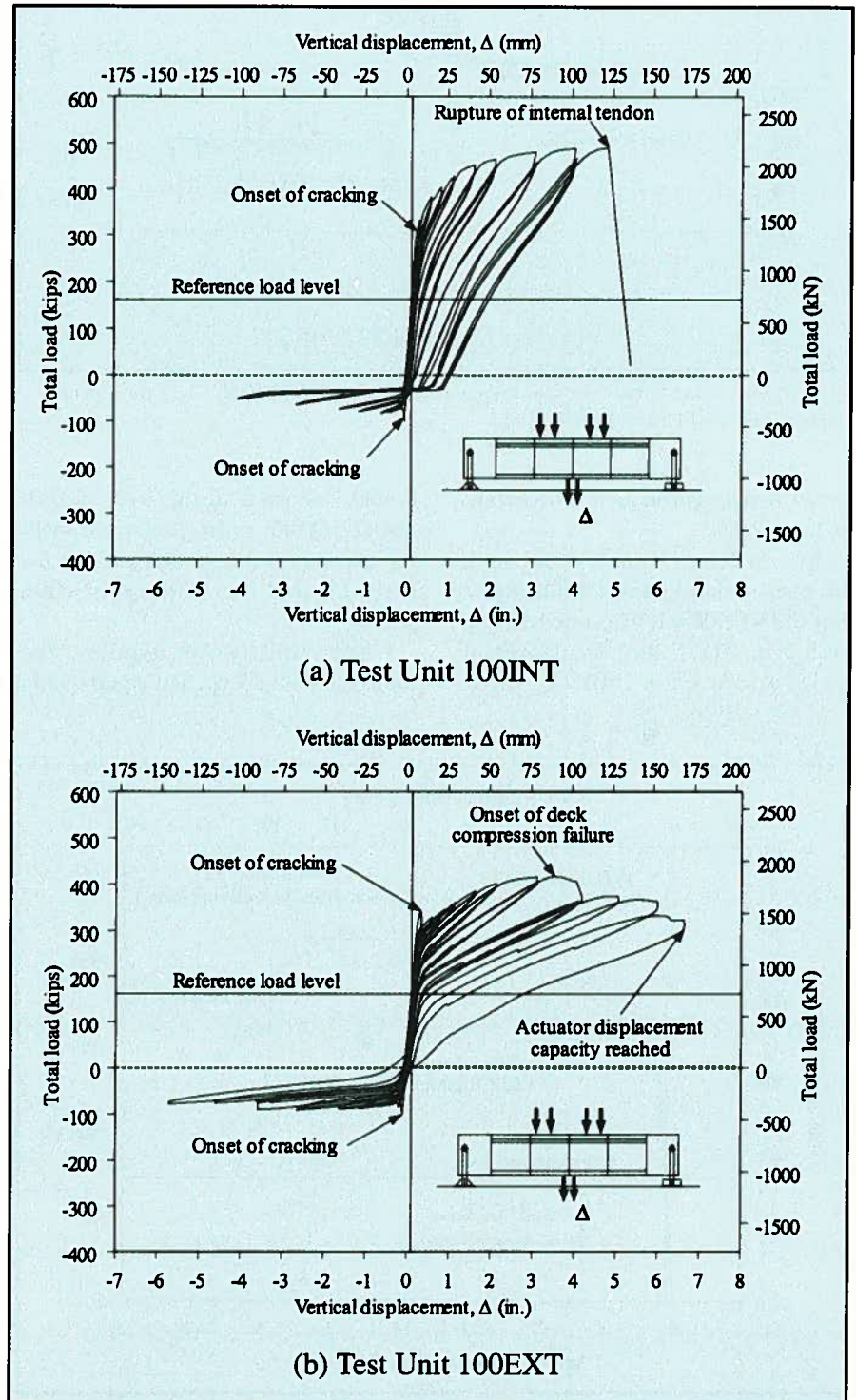


Fig. 7. Load versus vertical displacement measured at 6 in. (152 mm) from midspan: (a) Test Unit 100INT and (b) Test Unit 100EXT.

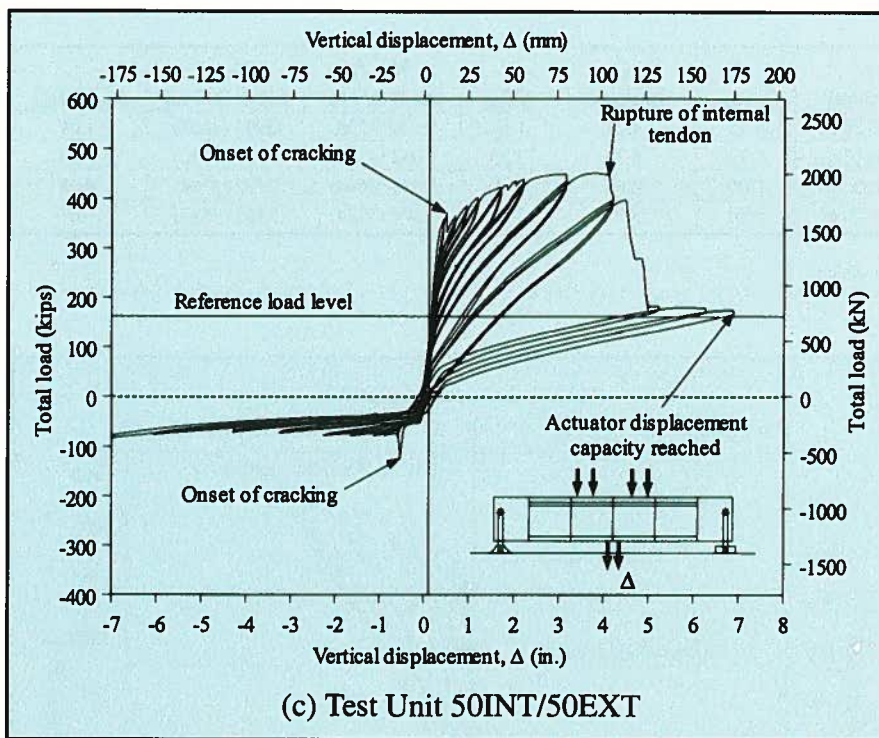


Fig. 7 (cont.). Load versus vertical displacement measured at 6 in. (152 mm) from midspan: (c) Test Unit 50INT/50EXT.

occurred during subsequent downward loading cycles.

Midspan Joint J3 was the only joint that opened during upward loading of Unit 50INT/50EXT. It opened during the 0.5 in. (12.7 mm) displacement cycle. As in Unit 100INT, shear

cracks occurred in the web of Unit 50INT/50EXT under downward loading between the supported ends of the test unit and the load application points.

Under downward loading, the midspan Joint J3 opened significantly

with increased applied displacement until rupture of some of the internally bonded tendon strands occurred at the midspan joint at a displacement of 4.1 in. (104 mm) and a peak load of 452 kips (2011 kN). Fig. 6c shows the midspan joint at onset of failure of the internally bonded tendon in Unit 50INT/50EXT.

During the 5.0 in. (127 mm) displacement cycle, more internally bonded strands ruptured accompanied by a significant drop in the load. The test continued for two displacement cycles after this, with only the external tendons intact.

Table 3 summarizes the experimental peak loads and maximum displacements of all test units, including Unit 100INTCIP of Phase I-A, under downward loading. In Table 3, P_u is the peak total load and Δ_u is the maximum displacement measured at 6 in. (152 mm) from midspan. Other experimental results given in Table 3 will be explained in a following section.

Load-Displacement Response

Fig. 7 shows the history of total applied load versus vertical displacement, measured at 6 in. (152 mm) from midspan for the Series I-B (Phase I-B) test units. The sign convention in Fig. 7 is positive for downward loading and displacement. Fig. 7 indicates that performance of Test Series I-B units was similar under upward loading. All of the test units failed under downward loading, as mentioned in the previous section.

The load-displacement envelopes for all test units, including Unit 100INTCIP of Phase I-A, are plotted in Fig. 8, for downward loading direction only, to enable comparisons of load-displacement responses for the different test units. The maximum displacements, Δ_u reported in Table 3 for all test units, correspond to the load levels indicated by the solid circles shown in Fig. 8.

The following observations can be seen from Fig. 8:

1. All test units could undergo significant inelastic displacements before failure.
2. Failure of the test units with internally bonded tendons (Units 100INT,

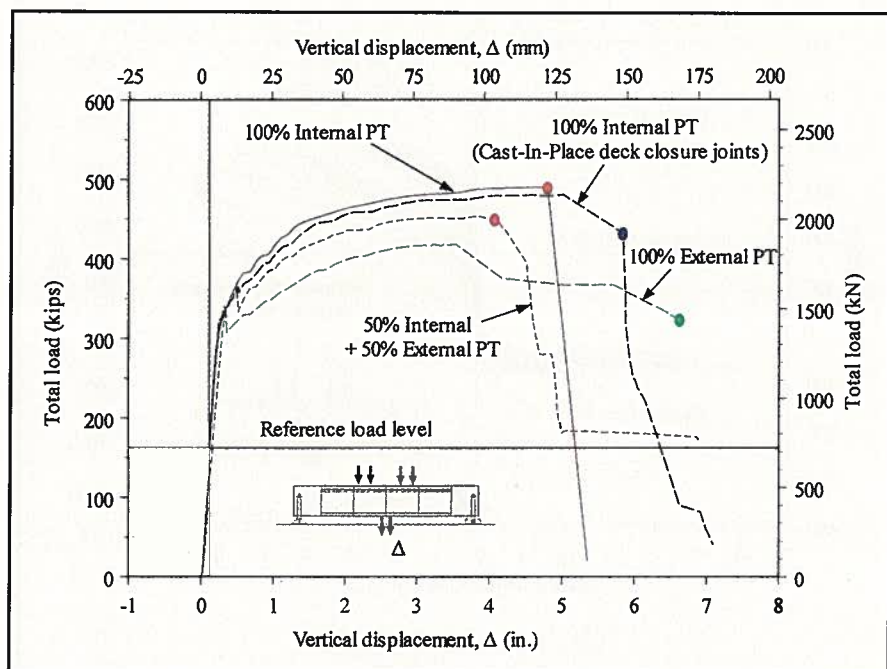


Fig. 8. Envelopes of load versus vertical displacement curves (downward loading direction only).

100INTCIP and 50INT/50EXT) was explosive. The load carrying capacity was completely lost upon failure of Units 100INT and 100INTCIP. A significant portion of the load carrying capacity of Unit 50INT/50EXT was lost upon rupture of the internally bonded tendon. However, Test Unit 50INT/50EXT had a residual load carrying capacity, which slightly exceeded the reference load level, because the external tendons were still intact.

3. Failure of Unit 50INT/50EXT occurred at a relatively low displacement compared to all other test units. The internally bonded tendon in Unit 50INT/50EXT was carrying significantly higher forces than the external tendons as will be shown later, resulting in relatively early rupture of the internal tendon. The curves shown in Fig. 8 indicate that a combination of internally bonded and external (unbonded) tendons, as currently allowed in the AASHTO Guide Specifications,¹ results in less desirable seismic performance.

4. Failure of Unit 100EXT was ductile, as the load carrying capacity dropped gradually with increasing displacements beyond the peak load. Unit 100EXT had the highest displacement capacity among all test units.

5. The load carrying capacity of Unit 100EXT was less than the capacities of the other test units because of lower stresses in the external tendons and because of the geometry change at midspan section due to the test unit's vertical displacement with the external tendons remaining essentially horizontal.

Flexural Moment Versus Opening of Joints

Opening of the joints occurred in the concrete cover adjacent to the epoxy layer between the bonded pre-cast segments, rather than in the epoxy layer itself.² As mentioned earlier, opening of all joints was measured by means of linear potentiometers. Examples of joint opening results are shown in Fig. 9, which shows joint opening at midspan (measured at the bottom surface) versus midspan flexural moment for the Phase I-B test units.

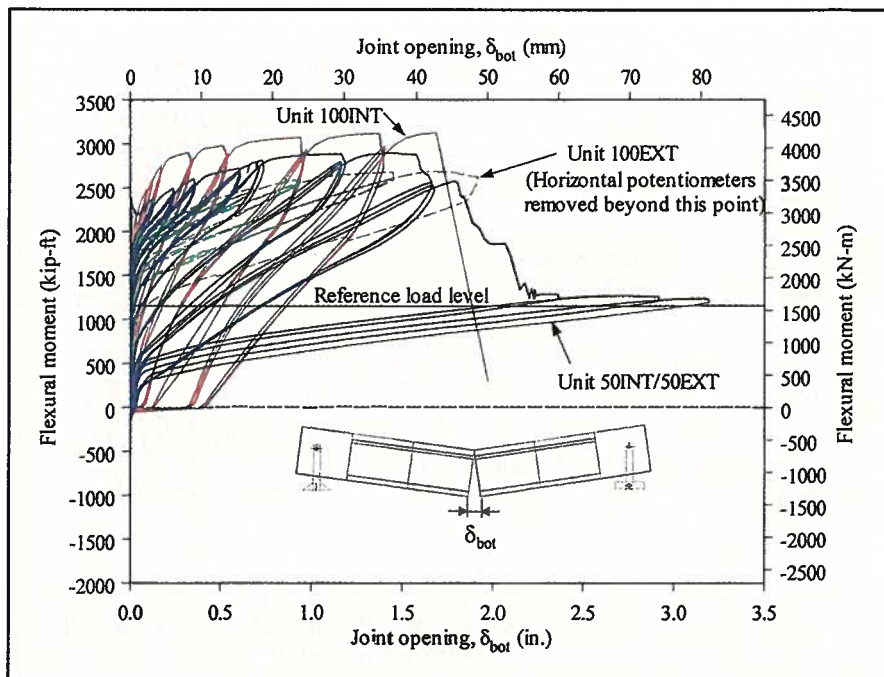


Fig. 9. Flexural moment versus midspan joint opening measured at the bottom surface (Phase I-B test units).

In any load-displacement cycle, permanent joint opening is that measured during unloading at the reference load level (represented by the horizontal solid line in Fig. 9). Fig. 9 indicates that Unit 100EXT had the lowest values of permanent joint opening among all test units. This indicates that with 100 percent external post-tensioning,

the joints will be closed almost completely following major seismic events.

Flexural Moment Versus Joint Rotation

Fig. 10 shows midspan joint rotation versus flexural moment for the

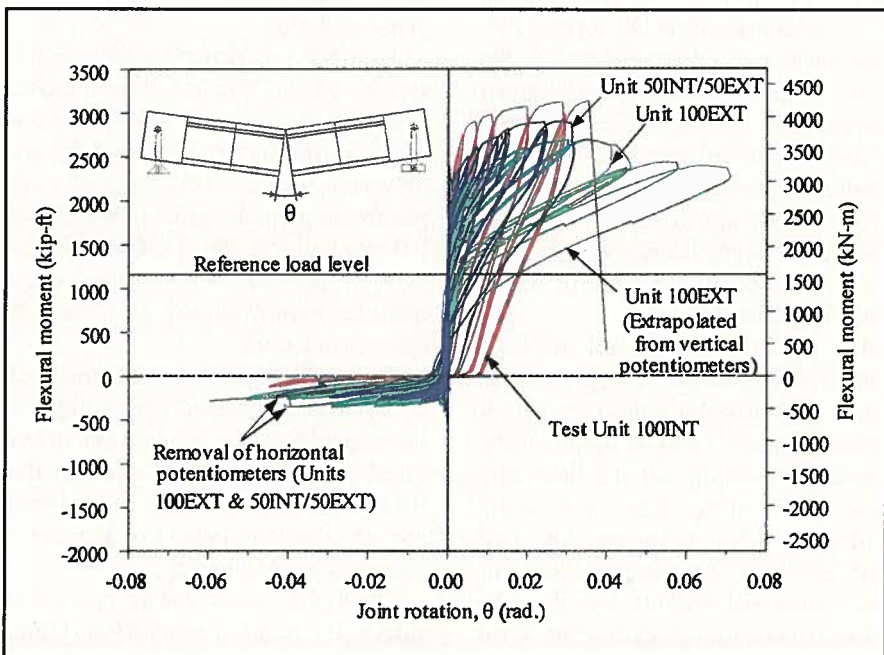


Fig. 10. Flexural moment versus midspan joint rotation (Phase I-B test units).

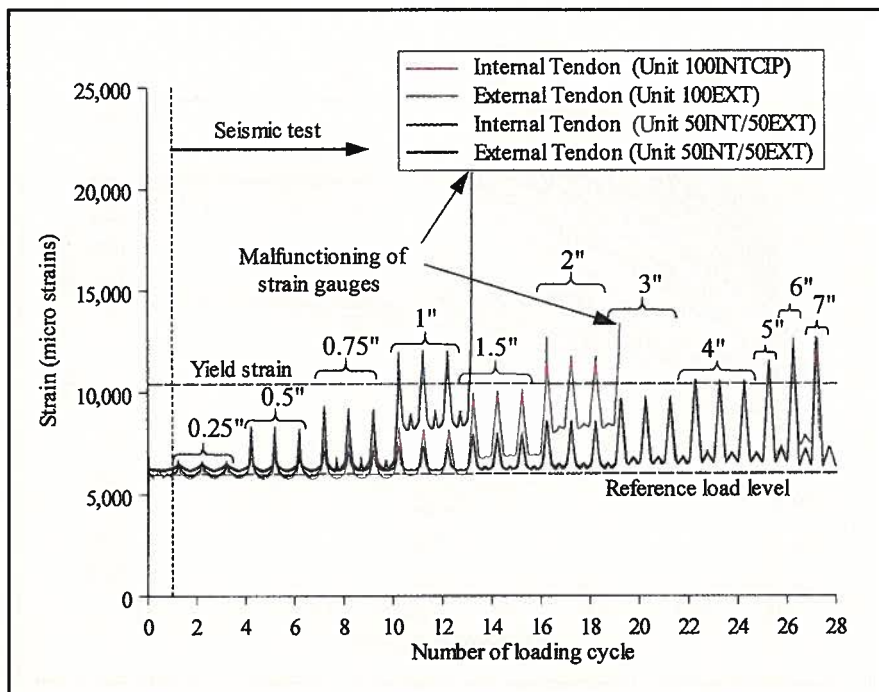


Fig. 11. Measured strains in the prestressing steel at midspan.

Phase I-B test units. The joint rotation was obtained from the joint openings measured at the top and bottom surfaces of the test units. The linear potentiometers that measured midspan joint openings fell off Test Units 100EXT and 50INT/50EXT during testing.

The potentiometers that measured joint openings fell off Unit 100EXT during the 5 in. (127 mm) displacement cycle; however, the joint rotation was extrapolated from the vertical displacements that were measured by the vertical potentiometers (see the green curve in Fig. 10). Fig. 10 indicates that with 100 percent external post-tensioning, rotational capacity of the joint could reach about 0.070 radians, which was significantly higher than the joint rotational capacity of all other test units.

The potentiometers fell off Unit 50INT/50EXT at the end of the 4 in. (102 mm) displacement cycle; it means just after onset of failure of the test unit by rupture of the internally bonded tendon. The maximum midspan joint rotation of Unit 50INT/50EXT was about 0.032 radians, which was slightly less than the joint rotational capacity of Unit 100INT with 100 percent internal post-tensioning.

Strains in Prestressing Steel

Fig. 11 shows the strain history measured at midspan Joint J3 in: (1) the internally bonded tendon in Unit 100INTCIP (Phase I-A), (2) one of the external tendons in Unit 100EXT, (3) the internally bonded tendon in Unit 50INT/50EXT, and (4) one of the external tendons in Unit 50INT/50EXT. Unfortunately, all strain gauges mounted on the prestressing steel of Unit 100INT were damaged during post-tensioning.

Although this paper focuses on the results of the Phase I-B test units, strains in the internally bonded tendon of Unit 100INTCIP (Phase I-A) are presented in Fig. 11 to compare with prestressing steel strains in the Phase I-B test units. In Fig. 11, Cycle 1 represents the time when strains were recorded before starting Test Stage II (the seismic test).

The yield strain level, represented by a horizontal dashed line in Fig. 11, corresponds to the 0.2 percent offset yield strain definition. Values of the maximum displacements at midspan are also shown in Fig. 11 on the corresponding loading cycles.

The figure shows that strains in the internally bonded tendons in Units 100INTCIP and 50INT/50EXT increased with applied loading until the

Table 4. Stresses in the external (unbonded) tendons at peak load.

Test unit	f_{ps} Eq. (1) ksi (MPa)	f_{ps} Test ksi (MPa)
100EXT	243.0 (1676)	245.5 (1693)
50INT/50EXT	243.0 (1676)	243.9 (1682)

strain gauges malfunctioned under downward loading. The strains recorded before malfunctioning of the strain gauges exceeded 0.013 and 0.020 in the internal tendons of Units 100INTCIP and 50INT/50EXT, respectively.

The following can be observed from the results shown in Fig. 11:

1. Significant plastic deformations of the internally bonded tendon in Unit 100INTCIP occurred during the 1.5 in. (38.1 mm) displacement cycles, whereas in Unit 50INT/50EXT plastic deformations in the internally bonded tendons started to occur at the relatively low displacement of 0.75 in. (19.1 mm). Also, the strain in prestressing steel increased with upward displacement and reduced after unloading to the reference load level (zero seismic displacement).

2. Plastic deformations of the external tendons occurred at substantially higher displacements than for internally bonded tendons.

3. The internally bonded tendon in Unit 50INT/50EXT carried a substantially higher force than the external tendons in the same test unit (see the strain plots for the two tendons in Fig. 11).

4. At the same midspan displacement levels, strains in the internally bonded tendon of Unit 50INT/50EXT were substantially higher than the strains in the internal tendon of Unit 100INTCIP. Joints J2 and J4 of Unit 50INT/50EXT (see Fig. 2 for joint numbers) had smaller rotations, at the same midspan displacement levels, than Joints J2 and J4 in Units 100INT and 100INTCIP. Thus, to get the same midspan displacements in Unit 50INT/50EXT, rotations of Joint J3 were relatively high compared to Units 100INT and 100INTCIP. This resulted in higher strains in the internally bonded tendon at midspan of Unit 50INT/50EXT. Also, the internal and external tendons in Unit 50INT/50EXT did not participate in

the force resistance in parallel but rather sequentially with the internally bonded tendon carrying most of the loading up to its failure.

5. The high strains and yielding of the internally bonded tendon at low displacements in Unit 50INT/50EXT indicate that for good seismic performance, combination of internally bonded and external (unbonded) tendons should be avoided in high seismic zones; the current AASHTO Guide Specifications¹ should be revised in this aspect.

Stresses in External (Unbonded) Tendons at Nominal Flexural Resistance

The experimental results showed that strains in the external (unbonded) tendons of Units 100EXT and 50INT/50EXT were less than strains in the internally bonded tendons. Reduction in strains and stresses of external unbonded tendons is considered in the AASHTO Guide Specifications,¹ which gives the following equation to calculate stresses in external tendons, f_{ps} , at nominal flexural resistance:

In U. S. units:

$$f_{ps} = f_{pe} + 900 \left(\frac{d_p - c_y}{\left(\frac{l_i}{1 + 0.5N_s} \right)} \right) \quad (\text{ksi}) \quad (1a)$$

In metric (SI) units:

$$f_{ps} = f_{pe} + 6207 \left(\frac{d_p - c_y}{\left(\frac{l_i}{1 + 0.5N_s} \right)} \right) \quad (\text{MPa}) \quad (1b)$$

where

- f_{pe} = effective stress in prestressing steel after losses
- d_p = distance from extreme compression fiber to centroid of prestressing steel
- c_y = neutral axis depth from the extreme compression fiber
- l_i = tendon length between anchorages
- N_s = number of support hinges crossed by the tendon

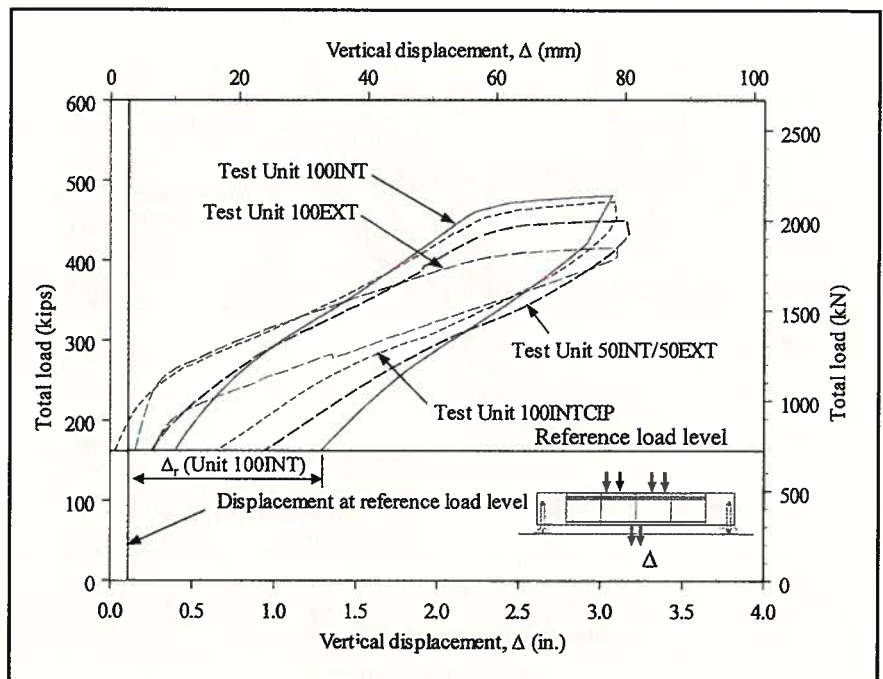


Fig. 12. Load versus vertical displacement for the 3 in. (76.2 mm) displacement cycle (downward loading direction only).

The effective stress, based on measured strains, at the beginning of the seismic test (Test Stage II) was about 181 and 179 ksi (1248 and 1234 MPa) in the external tendons of Units 100EXT and 50INT/50EXT, respectively. The second term on the right hand side of Eq. (1) gives the change in tendon stresses.

The AASHTO LRFD Bridge Design Specifications⁸ gives an equation similar to Eq. (1) to calculate f_{ps} ; however, the numeral 900 in the right hand side of Eq. (1a) is replaced by

913.5. Similarly, the numeral 6207 in Eq. (1b) is replaced by 6300.

According to the AASHTO LRFD Specifications,⁸ or when Eq. (1) is used, the stress in unbonded tendons should not be taken greater than the yield stress, f_{py} ($f_{py} = 0.90f_{pu}$ for low relaxation strands,⁸ where f_{pu} is the ultimate tensile stress). Values of f_{ps} calculated using Eq. (1), with $f_{ps} \leq f_{py}$, are given in Table 4 for the external tendons of Units 100EXT and 50INT/50EXT.

Strains in external tendons, ϵ_{ps} , at

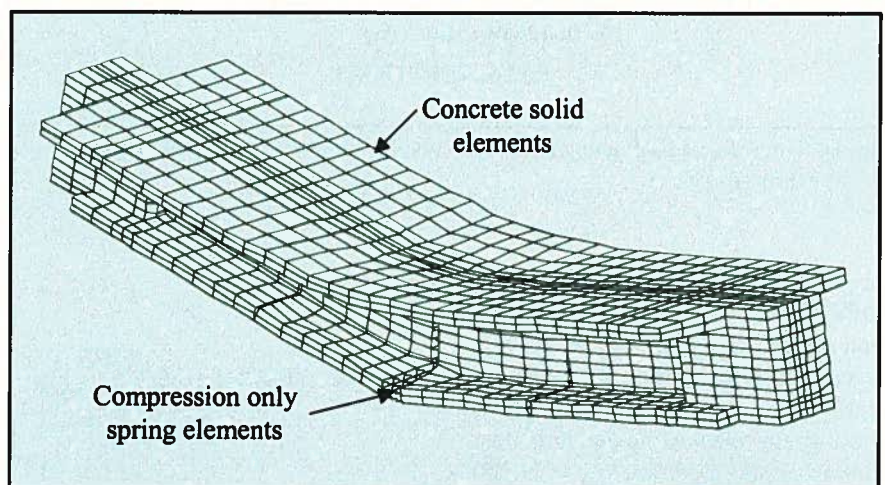
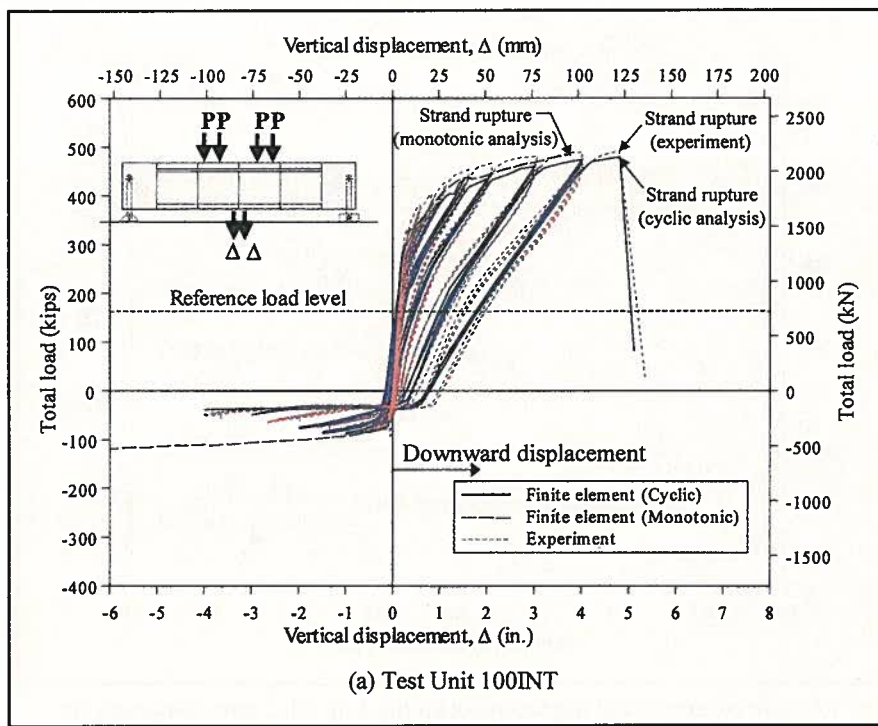
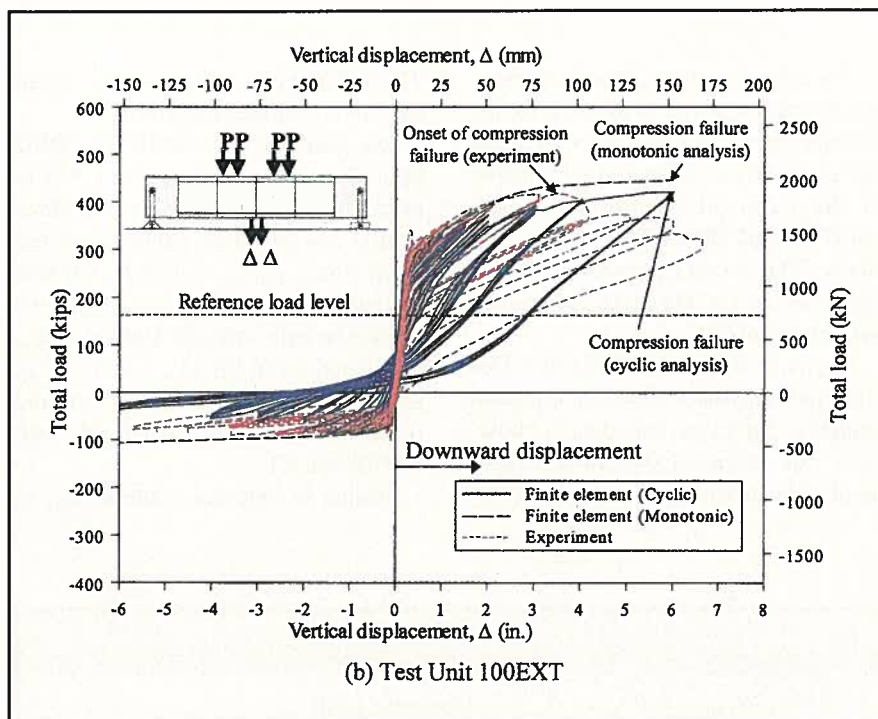


Fig. 13. Finite element model.



(a) Test Unit 100INT



(b) Test Unit 100EXT

Fig. 14. Load versus displacement analysis results: (a) Test Unit 100INT and (b) Test Unit 100EXT.

the peak load for Units 100EXT and 50INT/50EXT were measured. The tendon stresses, f_{ps} $_{Test}$, given in Table 4, were calculated from the measured tendon strains using the following stress-strain relationship equation⁹ (assuming elastic modulus, $E_{ps} = 29,000$ ksi = 200 GPa):

$$f_{ps} = 29,000 \epsilon_{ps} \left\{ 0.025 + \frac{0.975}{\left[1 + (118 \epsilon_{ps})^{10} \right]^{0.1}} \right\} \quad (2)$$

Table 4 indicates that the experimental values of tendon stresses were very close to those calculated using Eq. (1) given by the AASHTO Guide Specifications¹ (with $f_{ps} \leq f_{py}$). It should be mentioned that the yield stress upper limit on f_{ps} calculated using Eq. (1) was most likely inadvertently left out of the AASHTO Guide Specifications.¹

MacGregor et al.¹⁰ conducted an experiment on a three-span precast segmental box girder bridge model with external (unbonded) tendons. Eq. (1) is based on the method proposed by MacGregor et al.¹⁰ on prediction of stresses in unbonded tendons. Their test specimen was subjected to monotonic loading and not reversed cyclic loading. To the authors' knowledge, no previous experimental research has been conducted on the performance of precast segmental bridges under reversed cyclic loading.

Post-Earthquake Permanent Displacements

One important aspect for desirable seismic performance of bridges is to minimize permanent displacements of the superstructure after an earthquake event. Fig. 12 shows the applied load versus displacement during the downward loading portion of the 3 in. (76.2 mm) displacement cycle for all test units of Phase I.

The displacement, measured at the reference load level in the unloading portion of any of the curves shown in Fig. 12, represents the permanent displacement, Δ_r . Values of Δ_r measured after 3 in. (76.2 mm) maximum vertical displacement for all test units, are given in Table 3.

The values of Δ_r are normalized to the permanent displacement of Unit 100EXT, Δ_{Ref} ($\Delta_{Ref} = 0.14$ in. = 3.56 mm), and values of the ratio (Δ_r/Δ_{Ref}) are given in Table 3 for all test units. Comparison of the (Δ_r/Δ_{Ref}) values indicates that permanent displacements can be minimized by the use of 100 percent external post-tensioning. This is because strains in the external tendons are significantly less than strains in the internally bonded tendons (see Fig. 11).

The strains in external (unbonded)

tendons are spread over the whole tendons' length, whereas strains in bonded tendons are concentrated over a much shorter distance. Thus, for the same joint rotation, the strains in the bonded tendons are much higher than for the unbonded tendons. Inelastic strains in internally bonded tendons result in loss of the prestressing force, large permanent displacements and permanent joint openings.

Equivalent Viscous Damping Coefficient

The equivalent viscous damping coefficient, ζ , can be considered a measure of the energy dissipation capability of the test units. For comparison purposes, the coefficient ζ was determined by relating the area within the load-displacement hysteresis loop of the 3 in. (76.2 mm) displacement cycle to the elastic strain energy at the same cycle.¹¹ The values of ζ are given in Table 3 for all four test units of Phase I.

The equivalent viscous damping coefficients for all test units were normalized to that of Unit 100EXT, ζ_{Ref} ($\zeta_{Ref} = 2.63$ percent), and the ratios of (ζ/ζ_{Ref}) are given in Table 3. The values of (ζ/ζ_{Ref}) indicate that superstructures with internally bonded tendons are able to dissipate more energy than superstructures with external tendons.

Despite the enhancement in energy dissipation capability, use of cast-in-place deck closure joints (Unit 100INTCIP) may not be economical because they would complicate the precast segmental concept and would result in slower construction and higher costs. Also, energy dissipation capability is more important in the columns since column plastic hinging is anticipated whereas bridge superstructures are designed to remain essentially elastic during major seismic events. Thus, energy dissipation capability of the superstructure may not be an important design issue.

Flexural Moment Capacity

The experimental peak flexural moment at midspan, M_{Test} , is given in Table 3 for all four test units of Phase I. The calculated flexural moment ca-

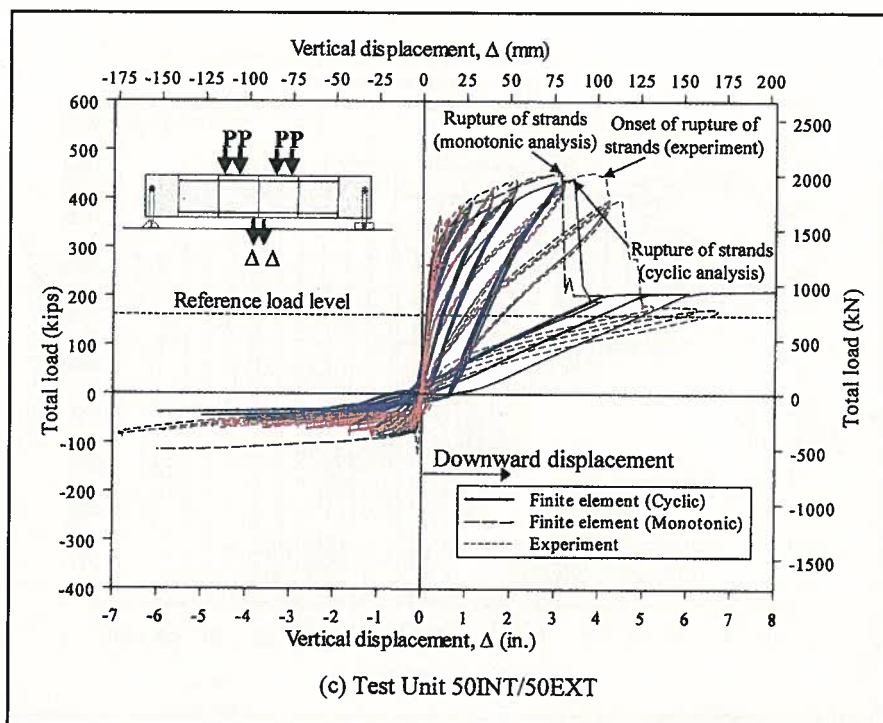


Fig. 14 (cont.). Load versus displacement analysis results: (c) Test Unit 50INT/50EXT.

capacity, M_{Calc} , as well as values of the ratio (M_{Test}/M_{Calc}) are also given in Table 3. The flexural moment capacity, M_{Calc} , was calculated according to provisions of Article 9.17 of the AASHTO Standard Specifications⁵ and Article 11.2 of the AASHTO Guide Specifications.¹ Stress in the external tendons at ultimate load was calculated using Eq. (1) according to provisions of Article 11.2 of the AASHTO Guide Specifications,¹ but assuming that the tendon stress would not exceed the yield stress, f_{py} ($f_{py} = 243$ ksi = 1676 MPa).

Values of the ratio (M_{Test}/M_{Calc}) were close to 1.00 for all test units, indicating that the flexural moment capacity of precast segmental bridge superstructures can be reasonably estimated using provisions of Article 9.17 of the AASHTO Standard Specifications⁵ and Article 11.2 of the AASHTO Guide Specifications.¹

The ratio (M_{Test}/M_{Calc}) was slightly less than 1.00 for Unit 100EXT, which had only external tendons. This slightly non-conservative estimate of flexural moment capacity for this test unit was due to the change in geometry of the cross section as the test unit was displaced vertically while the external tendons remained essentially

horizontal. This resulted in reduction of the internal moment arm between the tendons and centroid of the compressive stress block at the midspan section; this reduction in the moment arm was not considered in the calculation of M_{Calc} .

In calculating the flexural moment capacity of Unit 50INT/50EXT, stresses in the internally bonded tendons were different than stresses in the external tendons. Tendon stresses were calculated using provisions of the AASHTO Standard Specifications⁵ and the AASHTO Guide Specifications.¹

FINITE ELEMENT ANALYSIS

Three-dimensional finite element models of the test units were developed. The finite element models and results of Units 100INT and 100INT-CIP were presented in an earlier paper;² however, results of Unit 100INT will be briefly presented in this paper for completeness, and because Unit 100INT is one of the Phase I-B units.

Description of the Finite Element Models

Detailed finite element models were developed for all test units (Fig. 13).

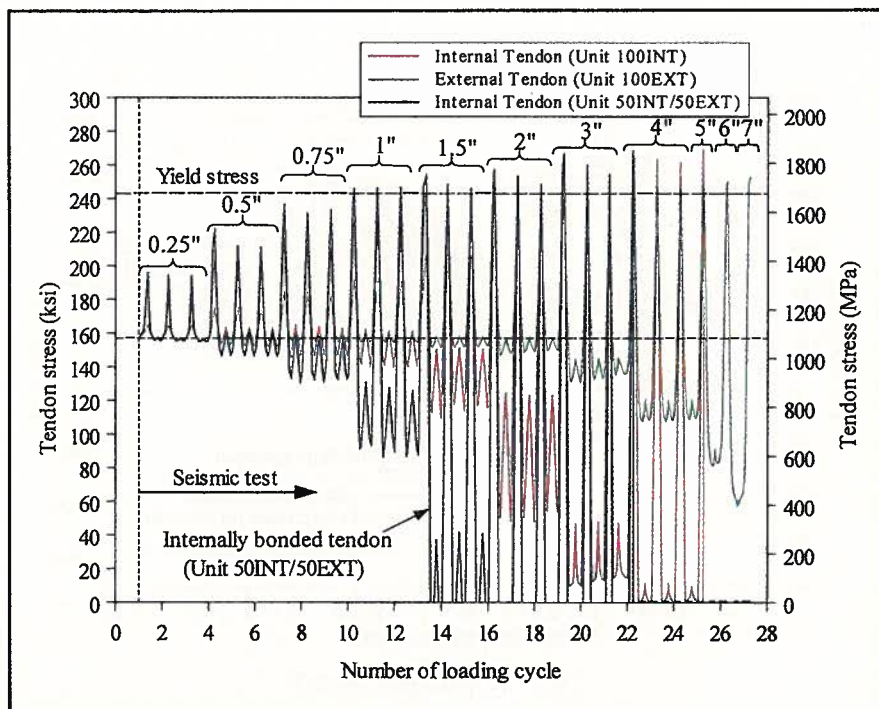


Fig. 15. Stress history analysis results of prestressing steel at midspan.

Analyses were performed using the general-purpose finite element program ABAQUS,¹² interfaced with the ANACAP¹³ concrete material model.

The concrete was modeled as 3-D, eight-node, solid brick elements with strain-hardening and strain-softening capabilities in compression, and tension cutoff with cracks that do not heal upon closure.¹³ Confinement effects were assumed to be negligible and the unconfined concrete strength was taken as 7.5 ksi (51.7 MPa). The model was developed in a similar way to the test units, with no solid elements crossing the joints between precast segments and no connection between solid elements on either side of the joints.

The joints were free to open by providing double nodes and compression-only springs at all nodes in the cross section at locations of joints. Prestressing steel was modeled by truss elements and connected to the concrete nodes at each 12 in. (305 mm) cross section, representing bonded strands.

External tendons were also modeled by truss elements, connected to the solid blocks in the precast end segments (Segments 1 and 6 in Fig. 2). Beyond 2.0 in. (50.8 mm) displacement in the upward loading direction,

the bottom slab of Test Units 100EXT and 50INT/50EXT was in contact with the external tendons; this contact was achieved by gap elements in the finite element models.

All mild steel reinforcement was modeled as 1-D sub-elements to the solid concrete elements. No mild steel reinforcement crossed the joints of Units 100INT, 100EXT and 50INT/50EXT. At the joints, the prestressing steel was not connected to the center nodes, but to nodes at sections 12 in. (305 mm) on either side of the centerline. This represented an idealized unbonded length at the joints of 24 in. (610 mm) and allowed for strain penetration on both sides of the joint. Loading was applied to the models in displacement control as shown in Fig. 5.

Finite Element Results

Test Unit 100INT — There was very close agreement between the analysis and measured load-displacement responses (see Fig. 14a). Analysis results showed that the model behaved very similarly to the test unit in terms of ultimate load, displacement at failure, and shape of the hysteresis loops in both the upward and downward loading directions. Rupture

stress and strain of the prestressing steel were assumed as 270 ksi (\approx 1860 MPa) and 0.04, respectively, which appeared to be reasonable based on Unit 100INT load-displacement results presented in Fig. 14a.

Fig. 15 shows the prestressing steel stress versus loading cycle number at midspan (Joint J3, see Fig. 2) from analysis of Test Unit 100INT. It is clear from Fig. 15 that beyond 0.75 in. (19.1 mm) displacement, plastic deformations of the tendon occurred and the initial prestressing force reduced significantly, and was completely lost following 4 in. (102 mm) of downward displacement.

Test Unit 100EXT — The shape of the monotonic load-displacement results for the upward loading direction matched the test results very well (see Fig. 14b). However, under downward loading, the monotonic load-displacement curve matched the test results only in the pre-peak range (see Fig. 14b). The failure mode was concrete crushing of the deck, as observed in the experiment. In the cyclic analysis, the model could not capture degradation of concrete strength with increased downward displacements and the failure mode according to the finite element analysis was crushing of the deck, as determined from strain contour values. The unloading stiffness of the analysis did not match that of the test very well.

Fig. 15 shows the prestressing steel stress versus loading cycle number at midspan (Joint J3, see Fig. 2) from analysis of Test Unit 100EXT. Fig. 15 shows that the external tendons yielded during the 3 in. (76.2 mm) first displacement cycle; the initial prestressing force started to reduce during the same displacement cycle but not dramatically, compared to the internally bonded tendon of Unit 100INT. The initial prestressing force was not completely lost, even at high midspan displacements through the end of the test.

Test Unit 50INT/50EXT — The cyclic load-displacement analysis results for Unit 50INT/50EXT matched the test results very well (see Fig. 14c). The shape of the monotonic load-displacement curve matched the test results only in the downward load-

ing direction. The failure mode from both monotonic and cyclic analyses was rupture of the internally bonded tendon, as observed in the experiment. The finite element model could reasonably capture the residual load carrying capacity of the test unit after rupture of the internally bonded tendon, as seen in Fig. 14c.

Fig. 15 shows the stress in the internally bonded tendon at midspan versus loading cycle number from analysis of Unit 50INT/50EXT. The figure shows that yielding of the internally bonded tendon occurred during the 1.0 in. (25.4 mm) displacement cycle, which was early compared to all other test units. This was due to the high force in the internally bonded tendon of this test unit as evidenced from the measured strains shown in Fig. 11.

The initial prestressing force started to reduce during the 0.75 in. (19.1 mm) displacement cycle and was completely lost after a maximum displacement of 1.5 in. (38.1 mm), which was again sooner than the other test units (see Fig. 15). This indicates that the combination of internally bonded and external tendons in high seismic zones may result in premature yielding of the internally bonded tendon and premature loss of the initial prestressing force. This may have important consequences in the design of precast structures, where under a severe earthquake the prestressing force is diminished or lost altogether before rupture of the strands.

DESIGN IMPLICATIONS

This paper presents the experimental and analytical results of Phase I of the research project on seismic performance of precast segmental bridges at the University of California at San Diego (UCSD). Seismic design recommendations can be made upon completion of the three phases of the research project. However, based on the results presented in this paper, the following can be implied for seismic design of precast segmental bridge superstructures:

- Combination of internally bonded tendons with external (unbonded) tendons, as currently allowed by the AASHTO Guide Specifications¹ may

result in premature yielding, loss of the initial prestressing force and rupture of the internally bonded tendons. In perspective of seismic design, combination of internally bonded and external tendons is not recommended.

- Use of only external tendons would improve the seismic performance in terms of ductility, displacement capacity, post-earthquake permanent displacements and permanent joint openings.

- The flexural capacity of precast segmental bridge superstructures is well-predicted using provisions of Article 9.17 of the ASSHTO Standard Specifications⁵ and Article 11.2 of the AASHTO Guide Specifications.¹ However, with external post-tensioning, designers should pay attention to the change in the internal moment arm between external tendons and the extreme compression fiber of the cross section. This change in moment arm should be considered in special cases such as in seismic design where large ductility and displacements are required in the superstructure. The stresses in the external tendons should not exceed the yield stress, f_{py} ($f_{py} = 0.90 f_{pu}$ for low relaxation strands⁸).

- Finite element analyses showed that the effective prestressing force in internally bonded tendons could reduce after a major seismic event, especially if the superstructure segment-to-segment joints are subjected to significant openings or rotations during the seismic event. External tendons proved to be a good alternative to internally bonded tendons in which case less reduction in the effective prestressing force is expected at high displacement levels.

CONCLUSIONS

A three-phase research project is currently in progress at the University of California at San Diego to investigate the seismic performance of precast segmental bridges. Results of a large-scale experimental program and finite element study of the seismic performance of segment-to-segment joints subjected to high flexural moments and low shears (Phase I) are presented in this paper. The following conclusions can be drawn from this study:

1. Crack patterns for all test units with internally bonded tendons were similar under downward loading. Only the midspan joint opened during testing of the unit with 100 percent external post-tensioning.

2. The segment-to-segment joints can experience significant repeated openings and closures under reversed cyclic loading without failure, even with no mild steel reinforcement crossing the joints. Precast segmental superstructures can undergo significant seismic displacements without failure.

3. Test Units 100INT and 50INT/50EXT experienced explosive failures as a result of rupture of the internally bonded tendon. With 100 percent external post-tensioning, the explosive failure was avoided and the load carrying capacity dropped gradually in Unit 100EXT with increased displacements in the post-peak range; the failure initiated by concrete crushing in the deck.

4. Ductility and displacement capacity can be substantially enhanced by use of 100 percent external post-tensioning. Use of only external tendons will also minimize post-earthquake permanent displacements of the superstructure as well as permanent openings of the segment-to-segment joints.

5. Combination of internally bonded and external (unbonded) tendons in precast segmental bridge superstructures, as currently allowed by the AASHTO Guide Specifications,¹ should be avoided in high seismic zones. This is because internally bonded and external (unbonded) tendons do not participate in the force resistance in parallel, but rather sequentially with the internally bonded tendons carrying most of the loading up to their failure.

6. Finite element analyses showed that under severe earthquakes, the prestressing force in the internally bonded tendons could diminish under repeated cycling in the inelastic strain range. Premature loss of the prestressing force may occur if internally bonded and external (unbonded) tendons are combined in the superstructure. Loss of prestressing force in external tendons is less severe for a given displacement or ductility level.

ACKNOWLEDGMENTS

Caltrans is acknowledged for funding this research under Contract No. 59A0051. Members of the AASHTO-PCI-ASBI Technical Research Committee are acknowledged for participating in the development of this research project.

J. Muller International, San Diego, prepared the construction drawings of the test units. Sika Corporation donated the

epoxy. Dywidag-Systems International (DSI), USA, donated the post-tensioning strands, high-strength bars and hardware.

The authors wish to express their appreciation to the PCI JOURNAL reviewers for their valuable and constructive comments.

REFERENCES

1. AASHTO, *Guide Specifications for Design and Construction of Segmental Concrete Bridges*, American Association of State Highway and Transportation Officials, Second Edition, Washington, DC, 1999.
2. Megally, S., Seible, F., Garg, M., and Dowell, R. K., "Seismic Performance of Precast Segmental Bridge Superstructures with Internally Bonded Prestressing Tendons," PCI JOURNAL, V. 47, No. 2, March-April 2002, pp. 40-56.
3. Megally, S., Seible, F., and Dowell, R.K., "Seismic Performance of Precast Segmental Bridges: Segment-to-Segment Joints Subjected to High Flexural Moments and High Shears," to be published in May-June 2003 PCI JOURNAL.
4. AASHTO-PCI-ASBI, *Segmental Box Girder Standards for Span-by-Span and Balanced Cantilever Construction*, American Association of State Highway and Transportation Officials, Precast/Prestressed Concrete Institute and American Segmental Bridge Institute, 1997.
5. AASHTO, *Standard Specifications for Highway Bridges*, 13th Edition, American Association of State Highway and Transportation Officials, Washington, DC, 1983.
6. Megally, S. H., Garg, M., Seible, F., and Dowell, R. K., "Seismic Performance of Precast Segmental Bridge Superstructures," Structural Systems Research Project Report SSRP-2001/24, Department of Structural Engineering, University of California at San Diego, La Jolla, CA, May 2002, 317 pp.
7. ASBI, *Recommended Contract Administration Guidelines for Design and Construction of Segmental Concrete Bridges*, American Segmental Bridge Institute, Phoenix, AZ, March 1995, pp. 109-116.
8. AASHTO, *LRFD Bridge Design Specifications*, Second Edition, American Association of State Highway and Transportation Officials, Washington, DC, 1998.
9. Collins, M. P., and Mitchell, D., *Prestressed Concrete Structures*, Response Publication, Toronto, Canada, 1997.
10. MacGregor, R. J. G., Kreger, M. E., and Breen, J. E., "Strength and Ductility of a Three-Span Externally Post-Tensioned Segmental Box Girder Bridge Model," Research Report 365-3F, University of Texas at Austin, Austin, TX, January 1989, 324 pp.
11. Chopra, A. K., *Dynamics of Structures*, Prentice Hall, Inc., Upper Saddle River, NJ, 1995, 729 pp.
12. Hibbitt, Karlson, and Sorenson, *ABAQUS User's and Theory Manual*, Version 5.8, 1999.
13. ANATECH Consulting Engineers, *ANACAP-U User's and Theory Manual*, Version 2.5, 1997.